Mapping the Agulhas Current from space: An assessment of ASAR surface current velocities

M. J. Rouault, Alexis Mouche, Fabrice Collard, J. A. Johannessen, Bertrand Chapron

Mapping the Agulhas Current from space: An assessment of ASAR surface current velocities

M. J. Rouault,[1,2] A. Mouche,[3] F. Collard,[3] J. A. Johannessen,[4,5] and B. Chapron[6]

Received 14 December 2009; revised 9 April 2010; accepted 17 June 2010; published 12 October 2010.

[1] Over 2 years of surface current information collected in the Agulhas Current region and derived from the Doppler centroid anomalies of Envisat's advanced synthetic aperture radar (ASAR) are examined. The sources of errors and potential use of ASAR surface current velocities for oceanographic research are assessed. ASAR surface current velocities are compared to surface drifter data and merged altimetry observations. Maps of sea surface temperature are used to establish the ASAR's capacity to capture the synoptic circulation. Discrepancies between observed and predicted ASAR velocities result predominantly from inadequate wind corrections combined with radar incidence angles below 30°. Occasionally observed wind-induced outliers cause a bias in the estimated ASAR velocities but do not affect the ability of the ASAR to systematically image regions of strong surface current flow and shear. Time-averaged maps of ASAR-derived surface current velocity seem able to accurately capture the position as well as the intensity of the Agulhas Current. The ability of the ASAR to pick up the smaller features of the circulation along the shelf break also shows that variability along the Agulhas Bank is of the same order of magnitude as that observed in the Agulhas retroflection. ASAR surface current velocities offer a very good complement to altimetry in regions where the mean dynamic topography is poorly resolved. The quasi-synoptic nature of ASAR acquisitions combined with the relatively high resolution of ASAR surface current velocities also make it attractive for studies of submesoscale processes and western boundary current dynamics.

Citation: Rouault, M. J., A. Mouche, F. Collard, J. A. Johannessen, and B. Chapron (2010), Mapping the Agulhas Current from space: An assessment of ASAR surface current velocities, *J. Geophys. Res.*, *115*, C10026, doi:10.1029/2009JC006050.

1. Introduction

[2] Measurements of current speed are essential to estimate the global transport of salt and heat which regulates our world's climate. At a regional scale, currents have a profound impact on the coastal and shelf ecosystems of the world and a thorough understanding of their strength and variability is necessary to monitor environmental change, maintain safety at sea and support shipping, fishing and offshore prospecting activities. In situ observations, while extremely accurate in defining the properties of ocean currents and their variability, are generally limited in their spatial and temporal coverage due to their high cost and the risk associated with the deployment of current moorings, especially in regions of intense flows. For more than two decades, satellite remote sensing observations have provided a cost-effective means of monitoring ocean surface currents. In particular, altimetry, through the use of the geostrophic approximation, has enabled scientists to estimate the upper transport and magnitude of the world's major ocean currents, track eddies or even discover new currents [*Siedler et al.*, 2006]. Closer to the shore however, altimetry suffers from serious limitation due to factors such as land contamination, atmospheric errors or inaccuracies in the estimation of the mean dynamic topography (MDT), which result in the loss of data typically 50 km from the coast [*Vignudelli et al.*, 2008; *Madsen et al.*, 2007]. In coastal and shelf regions, high-resolution Sea Surface Temperature (SST) and chlorophyll data sets have been used successfully to provide estimates of current speeds [*Emery et al.*, 1991]. Unfortunately, such methods suffer from the constant data loss caused by cloud cover and are inherently limited in isothermal regions. *Chapron et al.* [2005] proposed a new technique to extract surface current information from synthetic aperture radar (SAR) imagery, which could provide a means of mapping ocean currents from the open ocean to the coast at a high resolution, independent of cloud conditions. The method of *Chapron et al.* [2005], further referenced here as the Doppler

[1]Ecosystem Earth Observation, Council for Scientific and Industrial Research, Cape Town, South Africa.
[2]Oceanography Department, University of Cape Town, Cape Town, South Africa.
[3]Direction of Radar Applications, CLS, Plouzané, France.
[4]Nansen Environmental and Remote Sensing Center, Bergen, Norway.
[5]Geophysical Institute, University of Bergen, Bergen, Norway.
[6]IFREMER, Plouzané, France.

0148-0227/10/2009JC006050

shift method, relies on the careful analysis of the Doppler centroid anomaly; the anomaly accounting for the motion of surface roughness elements on the ocean surface corrected for the rotation of the earth, and enables one to derive estimates of the surface current velocity in the line of sight of the radar. Since July 2007, maps of surface current velocities in the Agulhas Current region have been systematically recovered from the Doppler shift measurements of Envisat's ASAR, under the European Space Agency (ESA) funded SAR ocean wind-wave-current project [*Collard et al.*, 2008; *Johannessen et al.*, 2008]. The Agulhas Current provides an ideal natural laboratory to test new remote sensing products such as the ASAR range-directed surface current velocities. With a mean transport of about 70 Sverdrup (1 Sverdrup = 10^6 $m^3.s^{-1}$) and surface current speeds at times greater than 2 m s^{-1}, the Agulhas Current constitutes the strongest western boundary current of the Southern Hemisphere, if not of the world [*Bryden et al.*, 2005]. The Agulhas Current can be divided into three regions, namely the northern Agulhas Current, the southern Agulhas Current and the Agulhas retroflection [*Lutjeharms*, 2006]. Each of these three regions is associated with different oceanographic processes and variability. It is in the northern Agulhas Current that the strongest flows are observed with mean maximum velocities of about 1.5 m s^{-1} [*van der Vaart and de Ruijter*, 2001] and a current core flowing very close to the shore [*Bryden et al.*, 2005]. The northern Agulhas Current is also singular in that it displays remarkably little variability [*Grundlingh*, 1983]. The oceanography of the southern Agulhas Current region is reminiscent of that associated with other western boundary currents and is characterized by a wide range of mesoscale and submesoscale processes such as rings, eddies, filaments or plumes [*Lutjeharms*, 2006]. The Agulhas retroflection region, where the Agulhas Current undergoes a sudden change of direction to become the Agulhas Return Current, has long been described as the region of highest variability in the Southern Hemisphere [*Cheney et al.*, 1983]. The complexity of the circulation in the Agulhas retroflection region has been widely documented [*Lutjeharms*, 2006] and is mainly dominated by the intermittent shedding of large Agulhas Rings and their associated secondary circulation. The range-directed surface current velocities derived from the ASAR provide a completely new type of information to the scientific community and offer a unique opportunity to further our understanding of the Agulhas Current system, particularly in regions where other remote sensing techniques might be challenged by factors such as land contamination, cloud coverage, isothermal flows or strong ageostrophic flows. This study assesses the ability of the ASAR velocities to capture the synoptic surface flow and illustrates how ASAR-derived surface current velocities can complement other remote sensing techniques to better portray the highly complex and variable dynamics of the Agulhas Current circulation. Section 2 of this paper introduces the data used for this research as well as the different methodologies followed. In section 3 the potential and limitations of ASAR range velocities are illustrated through comparisons with Lagrangian drifter observations and a model sensitivity study. The ability of both the ASAR velocities and the altimetry to represent the time-averaged circulation of the Agulhas Current system is addressed in section 3.3. At the end of section 3, two case studies are presented to illustrate the potential use of ASAR-derived velocities for oceanographic research. The conclusions of this study are drawn in section 4.

2. Data and Methods

[3] The region of study encompasses the greater Agulhas Current system, including the Agulhas Current proper, the Agulhas retroflection and the Agulhas Return Current and is defined as lying within 16°E–35°E and 23°S–43°S. Surface current velocities used in this study are derived from ASAR measurements as well as merged altimetry and Lagrangian drifters data sets. SST data are used to validate some of the observations seen in the altimetry and ASAR imagery. The SST data are collected from the Seviri instrument onboard the Meteosat Second Generation satellite and are processed by the French ERS Processing and Archiving Facility (CERSAT).

2.1. ASAR Current Measurements

[4] The principle of surface current measurements from the ASAR is similar to that of land-based radar measurement systems and involves the extraction of a line of sight velocity from information contained in the frequency spectrum of the returned radar echoes. The line of sight velocity can then be projected onto a horizontal plane to provide a range-directed surface current velocity. With precise information on the satellite's orbit and the antennae's attitude, it becomes possible to very accurately remove the effect of the motion of the satellite relative to the Earth from the Doppler spectrum. Over the ocean, the resulting Doppler anomaly thus contains information solely related to the motion of the sea surface roughness elements, which reflects the combined action of the wind, waves and current motions. Previous experiments using interferometry have demonstrated the ability of SARs to measure surface currents from airborne platforms [*Goldstein and Zebker*, 1987; *Shemer et al.*, 1993; *Romeiser et al.*, 2005]. *Chapron et al.* [2004] proposed a new methodology to derive surface current information from a single SAR antennae. Using the methodology of *Chapron et al.* [2004] and the Doppler centroid estimates provided by ESA in the metadata set of ASAR Wide Swath Medium (WSM) resolution images [*Madsen*, 1989; *Chang and Curlander*, 1992] (http://envisat.esa.int/handbooks/asar/CNTR2-6.htm#eph.asar.prodalg.levb.alg.descr.dopfreq), the radar division of Collecte Localisation Satellites (CLS) now processes all ASAR WSM images acquired over the Agulhas Current region on a systematic basis [*Collard et al.*, 2008; *Johannessen et al.*, 2008]. For each ASAR WSM acquisition, the Doppler centroid anomaly is extracted from the total Doppler centroid using a geometrical model. The Doppler centroid anomaly is then further processed to compensate along-track large cross section variations (induced by instrumental or signal processing errors) using land surface references. State of the art radar imaging models are required in order to precisely account for the relative influence of the wind, waves and currents on the mean motion of the sea surface roughness elements and its associated Doppler anomaly. Recent studies using both numerical [*Johannessen et al.*, 2008] and empirical models

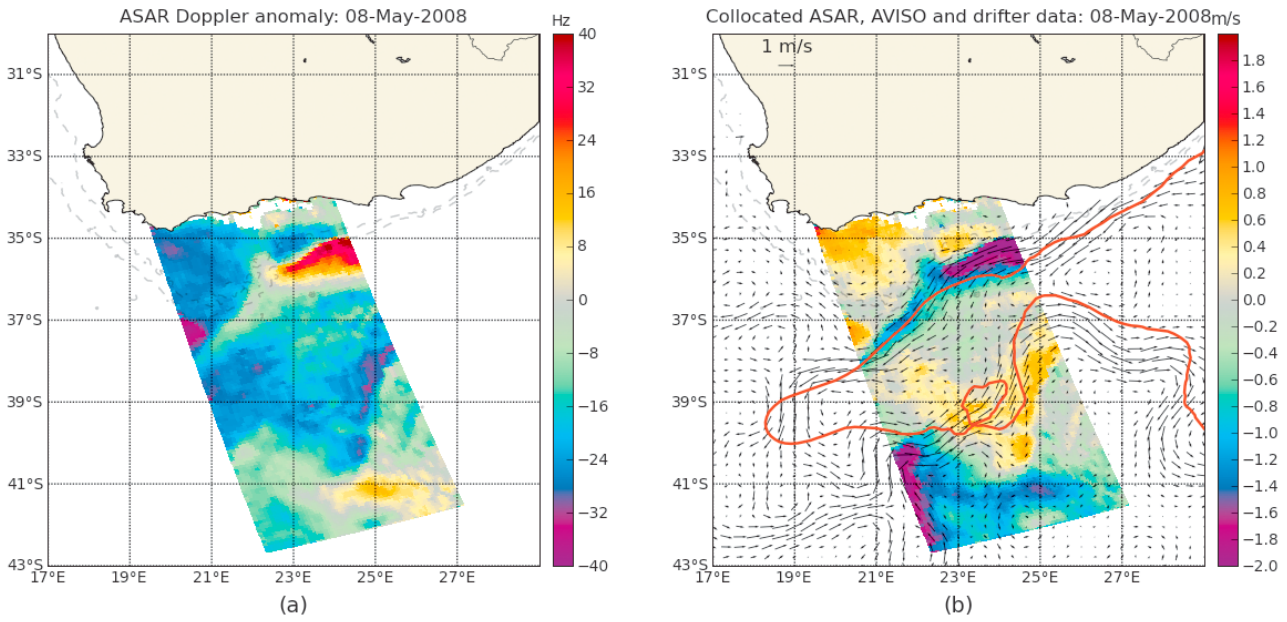

Figure 1. (a) Map of ASAR Doppler centroid anomaly (in Hz) corrected for large along-track cross-section variations and biases over land for 8 May 2008. (b) Resulting ASAR range-directed surface current velocity in m s^{-1}. Overlaid are vectors of geostrophic velocities derived by combining the CNES-CLS09 MDT with the AVISO NRT-MSLA product of that day. The trajectory of Lagrangian surface drifter 14926 between 9 June 2008 and 21 July 2008 is plotted as a red line. The stippled lines in Figures 1a and 1b indicate the positions of the 200 m and 100 m isobaths.

[*Collard et al.*, 2008] have shown promising results with range-directed surface current velocities determined with an RMS error equivalent to about 0.2 m s^{-1}. The ASAR surface current velocities presented in this paper were derived using the CDOP neural model network of *Collard et al.* [2008]. For each ASAR scene, European Centre for Medium-Range Weather Forecasts (ECMWF) reanalysis winds were used in combination with the CDOP model to predict all wave motion contributions dependent on the wind speed and direction, with the exception of wave-current interactions. Previous studies [*Mouche et al.*, 2008; *Johannessen et al.*, 2005] have shown that short-period waves contribute the most to the Doppler anomaly signal. Since these short waves quickly reach an equilibrium with the winds, most of their contribution to the Doppler anomaly is therefore removed when correcting for the influence of winds on the mean motion of sea surface roughness elements. The derivation of surface current velocities from the Doppler centroid anomaly can then be summarized as a three-step process: (1) calculating the Doppler centroid anomaly by removing the relative motion of the satellite to the Earth, (2) removing the wind-induced contributions from the total Doppler centroid anomaly and, (3) converting the Doppler centroid anomalies to range-directed surface velocities. The ASAR-derived velocities provide a measure of the absolute surface current velocity across the track of the satellite, with positive values indicating a flow moving away from the radar. In this study, the velocities derived from the ASAR data set are referred to as the ASAR range velocities. The ASAR range velocity product has a resolution of about 4 km in range and 8 km in azimuth [*Collard et al.*, 2008]. Over the Agulhas Current region, one descending (morning) and one ascending (evening) ASAR WSM image has been obtained every 3.5 days since July 2007. Near real-time range-directed surface current velocities derived from ASAR are freely available for download on the soprano Web site (http://soprano.cls.fr). An example of ASAR Doppler centroid anomalies and resulting range velocities acquired during one of Envisat's ascending path is given in Figure 1. Figure 1a shows a Doppler centroid anomaly map generated over the southern Agulhas region for 8 May 2008. The color plot in Figure 1b shows ASAR range velocities derived from the Doppler centroid anomaly map of Figure 1a, after wind-induced contributions have been removed. The negative surface current velocities (in the green to blue color range) indicate a flow toward the southwest, while positive velocities (in the yellow to red color range) indicate a northeasterly surface flow. Shades of green and blue along the Agulhas Bank clearly show the presence of the southward flowing Agulhas Current. The Agulhas Return Current is captured in shades of yellow, further south in the image. In this study, a total of 463 ascending and 358 descending ASAR WSM images collected between 2 August 2007 and 10 September 2009 were used.

2.2. Altimetry-Derived Current Measurements

[5] Sea surface height measurements related to the geostrophic approximation, provide a valuable tool for the characterization of the world's ocean circulation. Two particularly important measurements for oceanographers using altimetry data are the MDT and the sea surface height anomaly. The MDT, which is the difference between the mean sea level and the geoid, represents the influence of

permanent currents on the sea surface height, while the sea surface anomaly accounts for the currents variability. The absolute geostrophic current fields can then be recreated by adding the MDT to the sea level anomalies routinely measured by altimeters. The emergence of global MDT data sets [*Niiler et al.*, 2003; *Rio and Hernandez*, 2004; *Vianna et al.*, 2007] have provided oceanographers with a meaningful frame of reference for their sea surface height measurements. Over the last few years, MDT data sets have been combined with measurements of the sea level anomaly to estimate the absolute dynamic topography and its associated current fields. In this paper, we combine near real-time maps of sea surface height anomalies (NRT-MSLA) with the newly available CNES-CLS09 MDT of *Rio et al.* [2009] to produce maps of absolute geostrophic current velocity. The CNES-CLS09 MDT recently derived by *Rio et al.* [2009] was computed using a method similar to that described by *Rio and Hernandez* [2004]. The Mean Sea Surface (MSS) used for the derivation of the CNES-CLS09 MDT is calculated from a 7 year (1993–1999) mean of altimeter sea surface height measurements and a first-guess MDT is defined as the difference between the MSS and the geoid output from the GRACE gravity model. The initially low spatial resolution of the first-guess MDT ($\simeq$300 km) is improved through the assimilation of in situ observations and climatological data. The CNES-CLS09 MDT derived by *Rio et al.* [2009] is provided on a 1/4° resolution grid. The assimilation of extended data sets of drifting buoy velocities (1993–2008) and dynamic heights (1993–2007) into the CNES-CLS09 MDT significantly improves the portrayal of western boundary currents from altimetry [*Rio et al.*, 2009]. The NRT-MSLA product consists in a merged data set of the latest high-quality data produced from the OSTM/Jason-2, Jason-1 and Envisat altimeters. It is provided on a rectilinear grid with a spatial resolution of 1/3°. Both the CNES-CLS09 MDT and the NRT-MSLA products used in this study are available for download on the Archiving, Validation and Interpretation of Satellite Oceanographic data (AVISO) Web site (http://www.aviso.oceanobs.com). There are significant differences between SAR- and altimetry-based observations of surface current velocities. SAR observations provide a direct measurement of the surface current velocity in the radar range direction, while altimetry provides an indirect (geostrophy-based) measurement of the surface flow. In regions of invariant flow, the accuracy of the absolute surface geostrophic currents is therefore strongly dependent on the precision of the selected MDT. SAR and altimetry measurements also differ significantly in their temporal and spatial coverage. While altimetry benefits from a better global coverage, geostrophic currents derived from altimetry can only be obtained along the altimeter's track with repeat cycles varying between 10 and 35 days. As a consequence, both temporal as well as spatial interpolation are required to produce global maps of geostrophic currents. Although the synoptic representation of the surface circulation as shown in the AVISO data set is compromised by the spatial and temporal interpolation required to merge data from multiple altimeters, the NRT-MSLA product is the only data set available which allows direct comparison between the maps of the circulation captured with the altimeters and the ASAR, over the length of the ASAR data set.

2.3. Surface Drifter Current Measurements

[6] Surface Lagrangian drifter data processed in real-time mode by the Coriolis data assembly center (http://www.coriolis.eu.org/cdc/tsg_and_buoy_data.htm) are used to validate the ASAR range velocities. The Lagrangian drifters are surface floats equipped with a holey-sock drogue centered at 15 m. The data collected from such drifters are routinely processed and quality controlled by dedicated data assembly centers. Details of the quality control procedure for the real-time drifter buoys can be found in the Argo data manual. For our study, we downloaded all surface Lagrangian drifter data collected from 31 July 2007 to 23 April 2009. The criterion for the collocation of the drifter and the ASAR data sets was to retain all drifter data collected within 12 hours of the ASAR image acquisition and then to identify the drifters closest to the ASAR data points within a 5 km radius. After imposing our selection criteria for the ASAR collocations, a total of 53 drifters and 4215 collocations in the region of study were obtained. From these drifter data, only those of best quality and therefore associated with a flag value of 1 were retained. The drifter velocity observations were then projected to obtain a range-directed surface velocity directly comparable to that measured by the ASAR. Figure 1b illustrates how AVISO, drifter and ASAR observations of the surface circulation can be compared.

3. Results and Discussion

3.1. Comparisons Between ASAR and Lagrangian Drifters Velocities

[7] Direct comparisons between ASAR and drifters velocities provided an effective means of assessing the ability of ASAR range velocities to portray the flow dynamics. From 4215 collocations obtained mainly in the Agulhas Return Current region, the mean bias and RMS error between the ASAR and drifters range velocities was equal to 0.13 m s^{-1} and 0.56 m s^{-1}, respectively. It was found that the overall performance of the ASAR surface current velocities was negatively impacted by a few outliers. To illustrate the ability of the ASAR range velocities to represent the observed flow as well as highlight the main sources of discrepancies, we selected to focus our analysis on two drifters (14926 and 33681). Comparisons with drifter 33681 (Figure 2a) showed that the ASAR was able to capture regions of intense flow, with both the ASAR and drifters showing surface range velocities in excess of 1.7 m s^{-1}. The ability of the ASAR to capture strong currents was also apparent in comparisons made with drifter 14926 (Figure 2b). With drifter 14926 however, the initial bias and RMS error associated with the ASAR velocities were large due to a few outliers. A careful manual examination of the ASAR images used in the drifter 14926 analysis showed that some of the ASAR velocities outliers could be attributed to large rain cells being present at 3 of the collocated data points. Those points are plotted as diamonds in Figure 2b. For C band radars such as the ASAR, rain drops impinging on the sea surface can cause a local increase or decrease in the amplitude of the Bragg waves measured by the radar [*U.S. Department of Commerce*, 2004]. Such modifications of the Bragg wave spectrum can result in compromised Doppler

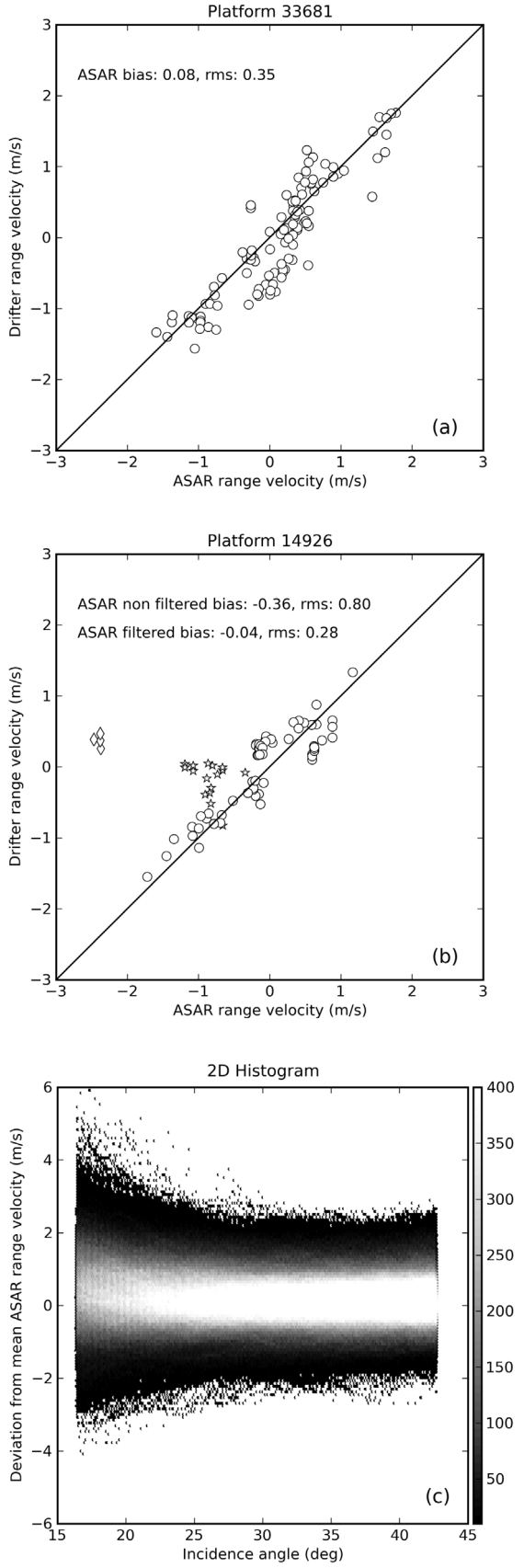

centroid estimates. In addition, the localized impact of rain cells on the local wind field [*Atlas*, 1994] is not captured in current global atmospheric models. In the presence of rain cells, the predicted Doppler shifts associated with the ECMWF winds will therefore be inaccurate and will further contribute to errors in the surface current velocities derived from the ASAR. Additional outliers in the ASAR range velocity, plotted as stars in Figure 2b, appear to all be associated with low radar incidence angles. In the CDOP neural network model mentioned in section 2.1, *Collard et al.* [2008] show that at low incidence angles, the returned radar echoes are stronger and dominated by larger and faster roughness elements. As a consequence, the contribution of vertical motions to the measured velocity increases at low radar incidence angles, making the extraction of a surface horizontal velocity from the Doppler centroid anomaly more challenging. The strong relationship between wind strength and short-period waves also implies that the relative impact of the wind on the Doppler anomaly increases with decreasing incidence angle. Due to the inverse relationship between the required wind correction on the Doppler anomaly and the radar incidence angle, inaccuracies in the predicted wind fields will induce larger errors in the ASAR range velocity at low radar incidence angles. Outliers associated with low radar incidence angles have a manifest impact on the ASAR range velocity data set, as shown in Figure 2c. Over the whole study region, deviations from the mean ASAR range velocity are for most data points confined to within 1 m s^{-1}, with few data points showing deviation from the mean in excess of 2 m s^{-1}. For incidence angles below 30° however, the ASAR range velocity bias strongly increases, with deviations from the mean sometimes in excess of 4 m s^{-1}. Although the range velocities derived from the ASAR are on occasion able to represent the measured flow with incredible accuracy, the overall performance of the ASAR range velocity product is negatively impacted by a few outliers. These outliers are predominantly encountered at low radar incidence angles and can be attributed mostly to inaccuracies in the predicted wind fields.

3.2. Sensitivity of ASAR Range Velocities to Inaccurate Wind Predictions

[8] The relationship between poorly predicted wind fields and errors in the ASAR range velocities can be better understood through a simple numerical experiment with the

Figure 2. Comparisons between the range-directed component of the ASAR and drifter surface current velocities (in m s^{-1}) for (a) drifter 33681 and (b) drifter 14926. In Figure 2b, diamonds indicate ASAR data points flagged because of large rain cells being present, while the stars are ASAR outliers resulting from inaccurate wind field predictions at low radar incidence angles (less than 30°). Flagged data points have not been included in the calculation of the mean and bias. (c) The two-dimensional histogram shows the relationship between the radar incidence angle and the deviation from the mean computed over the study domain. A larger number of outliers are observed at lower radar incidence angles.

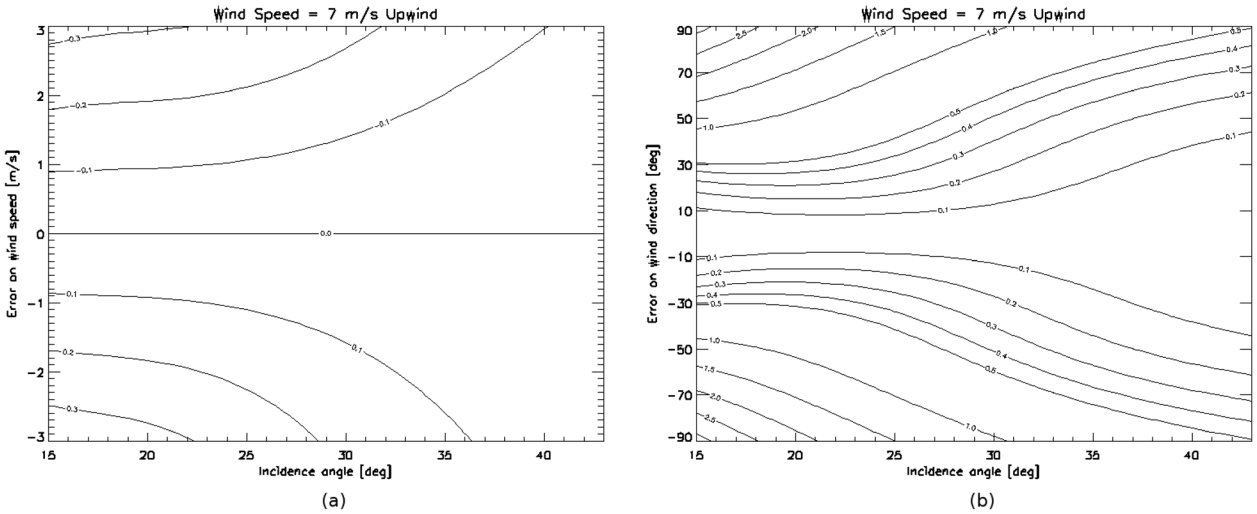

Figure 3. CDOP simulations illustrating the relationship between inaccurate wind field predictions and resulting error in the predicted ASAR surface current velocity, using reference winds blowing in an upwind configuration (toward the radar antenna) at 7 m s^{-1}. (a) Contour lines (in m s^{-1}) of the simulated error in range-directed surface current velocity as a function of the incidence angle (*x*-axis, in °) and wind speed errors (*y*-axis, in m s^{-1}). (b) Contour lines (in m s^{-1}) of the simulated error in range-directed surface current velocity as a function of the incidence angle (*x*-axis, in °) and wind direction errors (*y*-axis, in °). Figures 3a and 3b show an increase in the ASAR surface current velocity error at low radar incidence angles. The ASAR surface current velocity errors are particularly sensitive to inaccuracies in the wind directions.

CDOP model developed by *Collard et al.* [2008]. In our experiment, we first predict the ASAR range velocity with the CDOP model, using a reference wind of 7 m s^{-1} blowing in an upwind configuration (toward the radar antenna). The CDOP model is then used once again to see how deviations in speed and direction from the reference wind affect the predicted range velocity of the surface current. Errors associated with inaccuracies in the input wind speed are plotted in Figure 3a, while errors associated with inaccuracies in the input wind directions are plotted in Figure 3b. For a constant wind speed, upwind events are associated with stronger Doppler anomaly signals than downwind events [*Collard et al.*, 2008]. The upwind scenario used in this model experiment therefore provides an upper-bound estimate of the ASAR range velocity error for a reference wind speed of 7 m s^{-1}. Comparisons between wind fields measured from scatterometers and those predicted from global atmospheric models such as ECMWF have shown typical wind speed differences of about 2 m s^{-1} and RMS errors of about 20° in the wind direction [*Stoffelen and Anderson*, 1997; *Portabella et al.*, 2002]. According to Figure 3, each of these wind-induced error would translate into a maximum error in the ASAR range velocity of about 0.2 m s^{-1}. What the model clearly highlights is the relationship between the ASAR surface current velocity error and the radar incidence angle. The outputs from the CDOP model corroborates the analysis outlined in Figure 2c, which showed a sudden increase in the ASAR range velocity error below radar incidence angles of 30°. This model experiment also reveals the sensitivity of the ASAR surface current velocity error to inaccuracies in the wind direction, with a potential for small errors in the wind direction to significantly reduce the accuracy of the estimated surface current velocity in the radar range direction. The results of the CDOP model experiment emphasize the need for accurate wind predictions or observations to precisely estimate the velocity of ocean surface currents from SAR observations. An alternative to using ECMWF wind reanalyses when processing ASAR range velocities would be to use wind vectors directly derived from the ASAR observations. But while the feasibility of recovering wind speed and directions from SAR observations has long been demonstrated [*Stoffelen and Anderson*, 1997; *U.S. Department of Commerce*, 2004], the systematic recovery of wind vectors from SAR imagery still presents significant challenges. The main difficulty lies in the retrieval of wind directions, which are needed to derive wind speed estimates. Several methods have been proposed to recover wind directions from SAR observations. These include using atmospheric forecast models, collocated scatterometers information or linear features in the SAR image [*Vachon and Dobson*, 1996; *Horstmann et al.*, 2004]. Current research efforts focusing on the retrieval of autonomous wind directions from SAR by combining sea surface roughness with Doppler information could significantly improve the accuracy of future SAR surface current velocity products. Based on Figure 2c and the results of section 3.2, one should be particularly vigilant on the accuracy of input wind fields when considering ASAR surface current velocities associated with radar incidence angles below 30°. For radar incidence angles greater than 30°, the performance of the ASAR range velocity is expected to be satisfactory. In section 3.3, maps of the mean

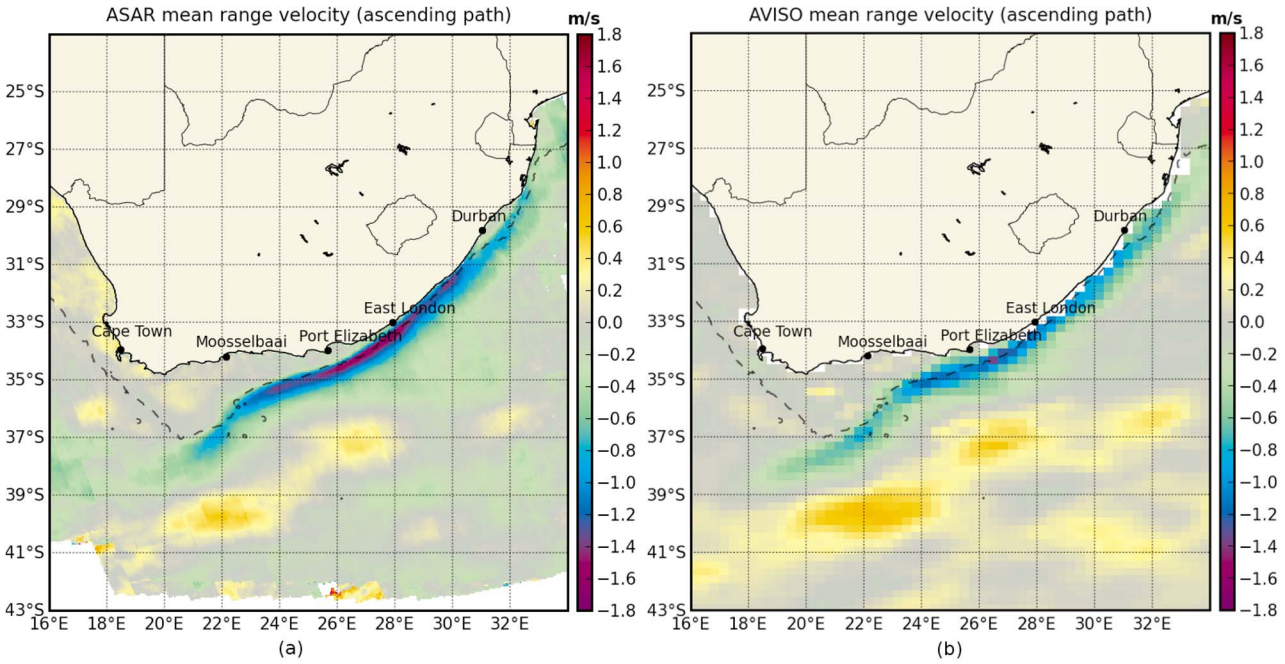

Figure 4. Mean range-directed surface current velocity (in m s^{-1}) in an ascending path configuration for (a) ASAR and (b) AVISO. Positive values indicate a flow toward the northeast, about 75° from the north. The ASAR mean was computed from 463 ASAR images collected over the Agulhas Current region from 2 August 2007 to 10 September 2009. Only data points with more than 10 observations and radar incidence angles greater than 30° were included in the calculation of the ASAR mean. AVISO current vectors were rotated in the ASAR-directed range velocity. The stippled black line in Figures 4a and 4b indicates the position of the 1000 m isobath.

range velocity computed from the AVISO and ASAR data sets are used to compare the ability of the remote sensing data sets to capture the mean circulation. ASAR range velocities at radar incidence angles below 30° are not included in the calculation of the time-averaged maps in an attempt to filter out outliers observed at low incidence angles.

3.3. Representing the Mean Circulation in the Agulhas Current System With ASAR- and Altimetry-Based Measurements

[9] Current velocities averaged over all ASAR ascending paths between August 2007 and September 2009 (Figure 4a) were used to illustrate the potential of ASAR range velocity measurements to portray the mean dynamics of the Agulhas Current. In an ascending path situation, the range velocities extracted from ASAR images are measured along an axis about 75° from the north and are roughly aligned with the main direction of propagation of the Agulhas Current. The velocities measured in the ascending path mode should therefore closely approximate the absolute speed of the Agulhas surface current. Maps of averaged range-directed surface current velocities computed for an ascending path configuration using both the ASAR and AVISO data sets (Figure 4), show that the mean position of the Agulhas Current, the position of its southern extension and the location of the Agulhas Return Current as represented by the AVISO data sets, agree well with those derived from the ASAR. The ASAR range velocities in the core of the Agulhas Current exceed those derived from the AVISO data sets. Near Port Elizabeth and in the core of the Agulhas Current, the range velocity derived from the ASAR is equal to 1.5 m s^{-1}, while that obtained by combining the CNES-CLS09 MDT with the AVISO NRT-MSLA is equal to 1.1 m s^{-1}. Peak range velocities in the Agulhas Return Current are similar for both the ASAR and AVISO data sets. The properties of the Agulhas Current as portrayed by the ASAR are consistent with those derived from hydrographic surveys and remotely sensed SST maps [*Bryden et al.*, 2005; *Lutjeharms*, 2006]. In the northern Agulhas region, the mean position of the Agulhas Current core as seen in the ASAR data set closely follows the 1000 m isobath, in agreement with that derived from a large number of hydrographic section [*Grundlingh*, 1983]. The mean range velocities derived from the ASAR corroborate the findings of *Pearce and Grundlingh* [1982], who estimated that mean annual current velocities in the northern Agulhas Current system varied between 1.4 m s^{-1} and 1.6 m s^{-1}, based on ship drift data. A parallel study (B. Chapron et al., manuscript in preparation, 2010) which collocates remotely sensed SST with ASAR range velocities, also shows a strong coherency between the position of the maxima in SST and the ASAR range velocity in the Agulhas Current, the Agulhas retroflection and the Agulhas Return Current regions, further confirming that the ASAR range velocities accurately position regions of intense flow. In the northern Agulhas region, the proximity of the current to the shore and its relatively invariant path make it very difficult for altimeters

to accurately capture the mean flow dynamics from sea level anomaly measurements. *Byrne and McClean* [2008] have shown that in the Agulhas Current system, the steric height dominates the sea level anomaly signal both at the low (less than 20 days) and high frequencies, due to the invariant nature of the current's path [*Grundlingh*, 1983]. As a consequence, in the Agulhas Current proper, an accurate estimate of the absolute geostrophic flow can only be achieved with a precise knowledge of the MDT. The use of the CNES-CLS09 MDT compared to the previously available Rio05 MDT of *Rio et al.* [2005] significantly improves the portrayal of the Agulhas Current dynamics from altimetry, increasing the peak Agulhas geostrophic current velocities in the Agulhas Current proper from about 0.5 m s^{-1} to over 1 m s^{-1} and enabling a better definition of the velocity gradient across the Agulhas Current (M. J. Rouault, personal observations, 2009). The CNES-CLS09 MDT of *Rio et al.* [2009] is a hybrid MDT, which makes use of extended data sets of drifting buoy velocities (1993–2008) and dynamic heights (1993–2007). In the Agulhas Current, where the MDT dominates the sea surface height signal, the time-averaged circulation obtained by combining the CNES-CLS09 MDT together with maps of sea level anomalies over the period 2007–2009 represents in reality a longer-term average due to the 15 years of in situ data assimilated in the CNES-CLS09 MDT. The time-averaged map of ASAR range velocities seems to accurately capture both the intensity as well as the position of the Agulhas Current. The finer spatial resolution of the ASAR data set improves the definition of the Agulhas Current's structure compared to that derived from altimetry. The ASAR range velocities provide a new, independent observation method, which could be used in the future to better monitor year to year changes in the Agulhas Current.

3.4. Using ASAR Velocities to Reveal Features of the Agulhas Current Circulation

3.4.1. Capturing the Submesoscale Circulation With the ASAR

[10] Some of the main advantages of SARs over other satellite remote sensing instruments is that they are able to image the ocean surface at a high spatial resolution, do not suffer from land contamination and can operate independently of cloud conditions. These characteristics make the SAR a promising sensor to study mesoscale and submesoscale processes (1 to 100 km) and interactions between western boundary currents and the coastal shelf regions. In section 3.4.1, we illustrate the ability of ASAR-based measurements to capture the smaller features of the circulation with a case study of shear edge instabilities detected on 27 February 2008. The surface circulation revealed by the ASAR on that date is compared to that depicted in AVISO and SST maps. In the second part of section 3.4.1, we reflect on how the ASAR's capacity to consistently image the submesoscale circulation can improve our understanding of the mean variability of the Agulhas Current system. ASAR range velocities measured on the 27 February 2008 are plotted as color contours in Figure 5a. Positive (yellow to red) range velocities indicate a surface flow toward the east-southeast while negative values (green to blue) are associated with a west-northwest surface flow. Overlaid are geostrophic current vectors obtained by combining the AVISO CNES-CLS09 MDT with the NRT-MSLA product for that day. Figure 5b shows the thermal signature of the surface waters derived from Seviri SST data collated over 26 and 27 February 2008. Two transect lines through the AVISO, SST and ASAR imagery have been extracted along the 20°E and 23°E longitudes. The positions of the transects are plotted as red lines in Figure 5a. Transect data appear in Figure 5c and Figure 5d. The 200 m and 1000 m isobaths are plotted as black lines on both Figure 5a and Figure 5b. The SST imagery provided an intuitive representation of the surface circulation around 27 February 2008. Surface waters with SST signatures of more than 23°C are plotted in shades of red in Figure 5b, and highlight the path of the Agulhas Current, the Agulhas retroflection (around 16.5°E and 41°S) as well as the Agulhas Return Current. The southward flowing Agulhas Current which roughly followed the 1000 m depth contour, the retroflection region as well as the circulation associated with the Agulhas Return Current were captured by both the ASAR and AVISO data sets in Figure 5a. There is a very good agreement between the patterns of surface circulation displayed in the SST and ASAR imagery. The maps of SST and ASAR range velocities both showed a widening of the Agulhas Current around 23°E, followed by a sharp bend southward at 21°E and a subsequent narrowing of the current between 21°E and 19°E (Figure 5a and Figure 5b). Large ASAR velocities were associated with strong gradients in SST, and regions of local SST maxima in the Agulhas Current coincided with the position of the Agulhas Current core depicted in the ASAR imagery (Figure 5c and Figure 5d). The surface circulation information derived by combining the CNES-CLS09 MDT and the NRT-MSLA was not able to highlight the localized widening or narrowing of the Agulhas Current, which was observed at 23°E and 21°E. In the transect extracted at 23°E (Figure 5d), the position the Agulhas Current as seen in the AVISO data sets also appeared too far inshore. The AVISO and ASAR data sets showed strong discrepancies for regions located inshore of the Agulhas Current. The ASAR range velocities highlighted two regions of cyclonic flow inshore the Agulhas Current and centered around 23°E, 36°S and 20°E, 37°S. In the merged altimetry, no flow was detected inshore the Agulhas Current at 20°E, while at 23°E the ASAR- and altimetry-derived surface velocities were in opposite directions. Altimeters can precisely measure anomalies in the sea surface height at a spatial resolution of about 7 km along the satellite's track and are therefore very capable of detecting small shear-edge eddies such as those observed in Figure 5. However, the temporal and spatial smoothing required to map geostrophic currents from multiple altimeters implies that small-scale or transient features of the circulation will be misrepresented in merged altimetry products such as the AVISO NRT-MSLA. At 23°E, ASAR range velocities showed the presence of a surface counter current extending 60 km inshore of the Agulhas Current and with a width of about 160 km. This eastward flowing surface current is plotted in shades of yellow to orange in Figure 5a. Although no well-defined warm water plume could be seen at the southward edge of the cyclonic meander, waters in the across shelf return flow had a distinct SST signature, with SST 1°C warmer than those encountered on the Agulhas

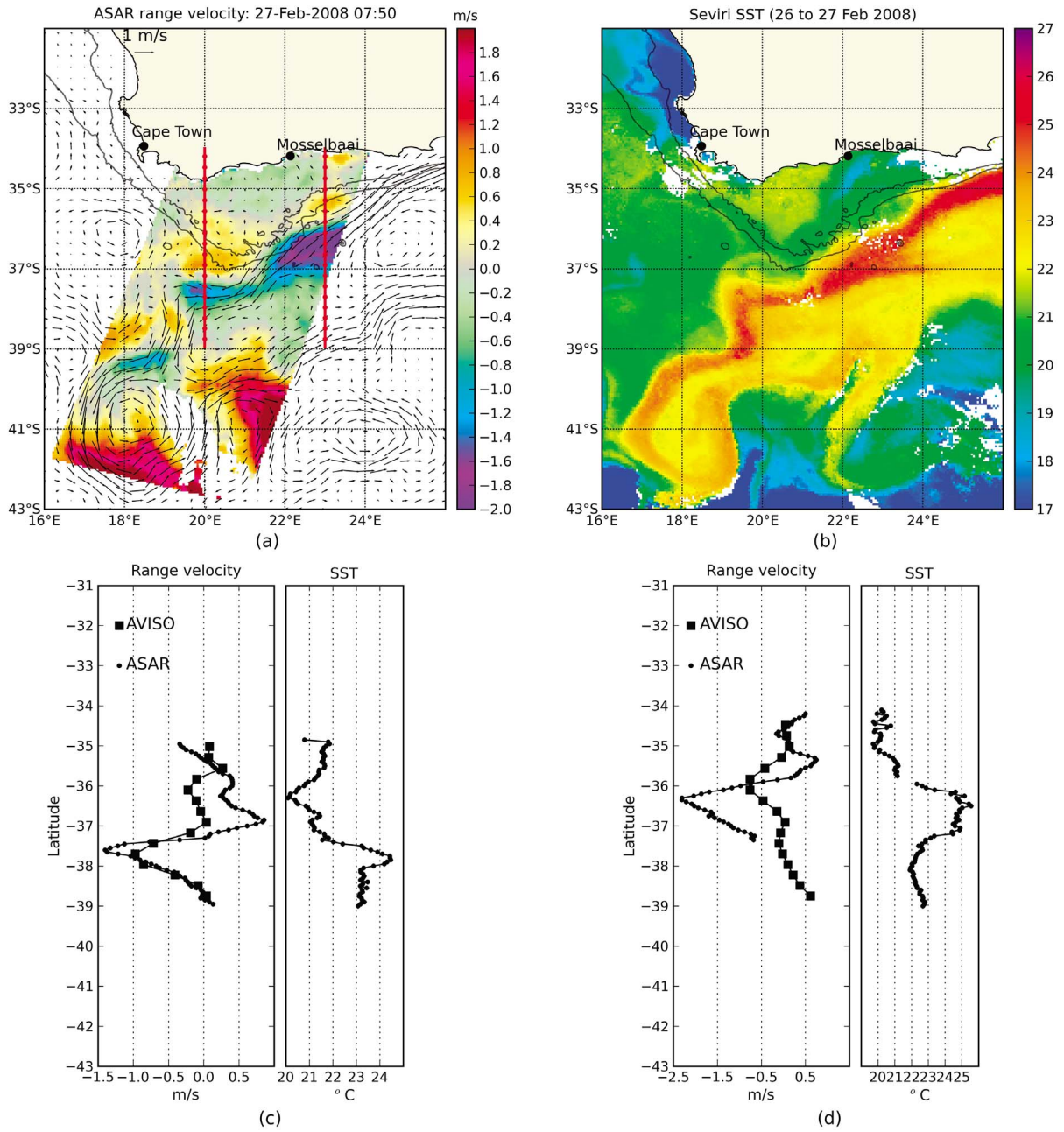

Figure 5. Regions of sharp cyclonic shear and SST gradient located inshore of the Agulhas Current at 23°E, 36°S and 20°E, 37°S evidenced by ASAR and SST data sets on 26 and 27 February 2008. (a) Color contours of ASAR range-directed surface current velocities (in m s^{-1}) with positive values (yellow and red) indicating an eastward flow. Overlaid are vectors of AVISO geostrophic currents on that same day. (b) The Seviri mean SST (averaged over 26 and 27 February 2008). (c and d) Transects of ASAR range velocity, AVISO range velocity, and SST extracted at 20°E (Figure 5c) and 23°E (Figure 5d) and plotted as red lines in Figure 5a. Solid black lines in Figures 5a and 5b indicate the position of the 200 m and 1000 m isobaths.

Bank and about 3°C cooler that those encountered in the Agulhas Current proper (Figure 5d). The maximum velocities measured by the ASAR in the counter current reached 0.7 m s^{-1}. The current velocities derived from ASAR around 23°E are thought to have been largely overestimated. Data points between 24°E and 22°E were coincident with low radar incidence angles and therefore subject to larger errors. The ASAR range velocity at 23°E and in the core of the Agulhas Current peaked to 2.3 m s^{-1}, a very high value in comparison to the 1 m s^{-1} previously observed [*Lutjeharms*, 2006] and modeled [*Penven et al.*, 2001] in the southern Agulhas Current. The relatively large width of the current at

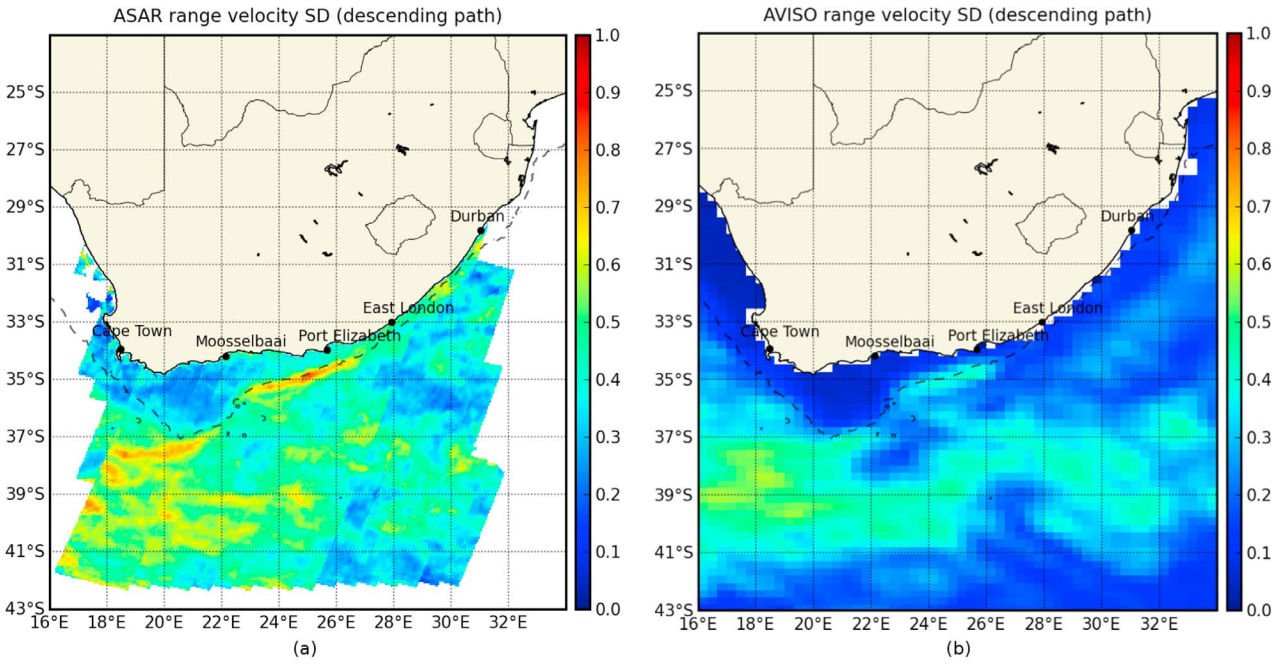

Figure 6. Standard deviation for (a) ASAR and (b) AVISO range-directed surface current velocities in a descending path configuration. The ASAR standard deviations were computed from 358 ASAR images collected over the Agulhas Current region from 2 August 2007 to 10 September 2009. Only data points with more than 10 observations and a radar incidence angle greater than 30° were included in the calculation of the ASAR mean. AVISO current vectors were rotated in the ASAR-directed range velocity to simulate a descending path situation. The stippled black line in Figures 6a and 6b indicates the position of the 1000 m isobath.

23°E and the fact that the ASAR range velocities were not aligned with the Agulhas Current flow would also imply that the ASAR range velocities around 23°E should have been well below the 2.3 m s^{-1} value. Despite the presumably erroneous values derived from the ASAR Doppler anomaly at these low incidence angles, the ASAR range velocity map still provided valuable information on the position of the Agulhas Current, its width and the existence of a surface counter flow along the continental shelf edge. It is worth noting that neither the SST nor the merged altimetry imagery provided evidence on the existence of the surface counter flow inshore of the Agulhas Current at 23°E. ASAR velocities at 20°E were coincident with high radar incidence angles (>30°) and roughly aligned with the main direction of propagation of the Agulhas Current. Therefore, the ASAR velocities around 20°E should presumably be more representative. Between the 23°E and 20°E longitudes, the distance between the Agulhas Current core and its northern edge decreased from 60 km to 30 km. The maximum ASAR range velocities at 20°E were equal to 1.4 m s^{-1} in the Agulhas Current and 0.9 m s^{-1} in the surface counter flow of the eddy. The meander centered at 20°E had a well defined SST expression, with a delineated plume of warm Agulhas water originating from the southern edge of the meander seen to loop back toward the current. Based on the SST map in Figure 5b, the circumscribed cyclonic border eddy measured approximately 80 km by 220 km along the north/south and east/west directions, respectively. This large border eddy was associated with relatively colder water (Figure 5c). Previous studies [*Harris et al.*, 1978; *Lutjeharms et al.*, 1989] have shown that shear-edge eddies start developing due to an increase in the meandering of the Agulhas Current past Port Elizabeth. The downstream growth in size and strength of the meanders eventually leads to the development of an instability at the leading edge of the meander. This instability takes the form of a warm water plume, which may disperse over the Agulhas Bank or turn toward the current to form a cyclonic eddy [*Lutjeharms*, 2006]. In situ as well as numerical experiments [*Lutjeharms et al.*, 2003; *Penven et al.*, 2001] have suggested that border eddies such as that observed by the ASAR at 20°E, eventually separate from the Agulhas Current to move westward into the South Atlantic Ocean. The detachment of these cyclonic eddies from the Agulhas Current has been attributed to the combined effect of the downstream advected cyclonic shear and the poleward termination of the Agulhas Bank, which eventually lead to the eddy separating through a flow detachment process [*Penven et al.*, 2001]. Border eddies such as those captured in the ASAR imagery of 27 February 2008 are common features of western boundary currents [*Koshlyakov*, 1986] and their impact on the productivity of coastal shelf waters has been clearly demonstrated [*Lee et al.*, 1981]. In the southern Agulhas, the ubiquitous presence of meanders and shear edge perturbations at the inshore edge of the current induces localized upwelling and contributes to the intensification of the ther-

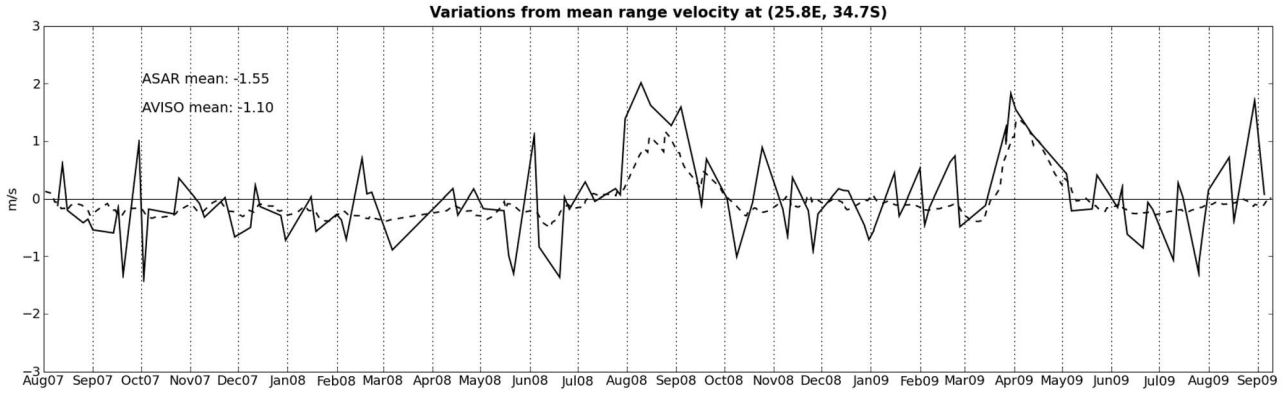

Figure 7. Fluctuations from the mean ASAR and AVISO range-directed surface current velocities (in m s^{-1}) at the position of the mean local maxima in the Agulhas Current core, offshore Port Elizabeth (25.8°E, 34.7°S). ASAR range velocities are derived for all ascending path observations collected between August 2007 and September 2009 and are plotted as a solid black line. The range-directed surface current velocities projected for ascending path configurations and calculated by combining the CNES-CLS09 MDT with the AVISO NRT-MSLA daily product are plotted as a dashed line. The largest anomalies in the ASAR and AVISO range velocities were observed in August 2008 and April 2009 and were associated with the passage of Natal pulses.

mocline on the Agulhas Bank through the input of warm Agulhas water in the upper layers [*Largier et al.*, 1992]. Shear edge eddies along the Agulhas Bank also contribute to the transport of Cape Anchovy larvae from the spawning ground of the eastern Agulhas Bank to the nursery grounds of South Africa's west coast upwelling system [*Probyn et al.*, 1995]. A proper quantification and understanding of the border shear edge eddies observed in the southern Agulhas Current is necessary to quantify the coastal shelf exchange as well as the interocean transport between the Indian and the Atlantic Oceans. Observation of sea surface height variability over the Indian Ocean have always portrayed the Agulhas retroflection and the Agulhas Return Current as the regions of maximum variability [*Cheney et al.*, 1983]. Those regions of high variability are also apparent in the AVISO standard deviation map of surface range velocities (Figure 6b). Using over 2 years of data collected over the Agulhas Current region with ASAR, we produced a map of the standard deviation for ASAR range velocities derived over all descending tracks. The descending track configuration lends itself well to capturing fluctuations in current speed at the northern edge of the Agulhas Current as it measures the intensity of the flow along a northwest/southeast axis (115° from the north). The ASAR map of the standard deviation in range-directed surface current velocities (Figure 6a) shows two lines of high variability along the Agulhas Bank between 23°E and 26.5°E and from the tip of the Agulhas Bank to the retroflection (from 18°E to 21.3°E). The ASAR data set shows that the variability along the Agulhas continental shelf between Port Elizabeth and Mossel Bay is just as high as that encountered in the Agulhas retroflection. In the standard deviation map produced from the AVISO data sets, increased variability along the Agulhas Bank is also observed but because the scales of variability along the Agulhas Bank are smaller, they are not always seen and are therefore underestimated. The high resolution of the ASAR data set also enables to differentiate between the intensity in variability along the shoreward and the seaward edges of the southern Agulhas Current, with most of the submesoscale activity occurring along the shoreward edge of the Agulhas Current. Standard deviation maps derived for ascending path ASAR configurations (not shown) confirm that the magnitude of the variability in the retroflection region and along the Agulhas Bank are comparable.

3.4.2. Imaging the Natal Pulse With the ASAR

[11] In an attempt to identify perturbations in the Agulhas Current over the sampling period, a time series of ASAR and AVISO range-directed surface current velocities was extracted at 25.8°E, 34.7°S, at a location which corresponds to the mean position of the Agulhas Current core, offshore Port Elizabeth (Figure 7). This time series was derived using all ASAR ascending path observations, when the surface velocity measured by the ASAR is closely aligned with the main direction of propagation of the Agulhas Current. Variations from the mean ASAR range velocities are plotted with a solid black line. The time series of ASAR range velocities at 25.8°E, 34.7°S showed rapid and large fluctuations over periods of a few days and throughout the measurement period. Whether these high-frequency fluctuations were real or due to "noise" cannot be tested due to the absence of in situ measurements in the region. The range velocities derived from the AVISO data sets did not display high-frequency modulations. This is due to the temporal as well as spatial smoothing required to produce merged maps of geostrophic currents from sea surface height measurements. Despite these differences, the ASAR and merged altimetry data sets were coherent in their identification of the largest perturbations in the Agulhas Current. Between August 2007 and September 2009 (Figure 7), two very large anomalies in the Agulhas Current were detected using the time series of AVISO and ASAR range velocities. These perturbations, which occurred around August 2008 and

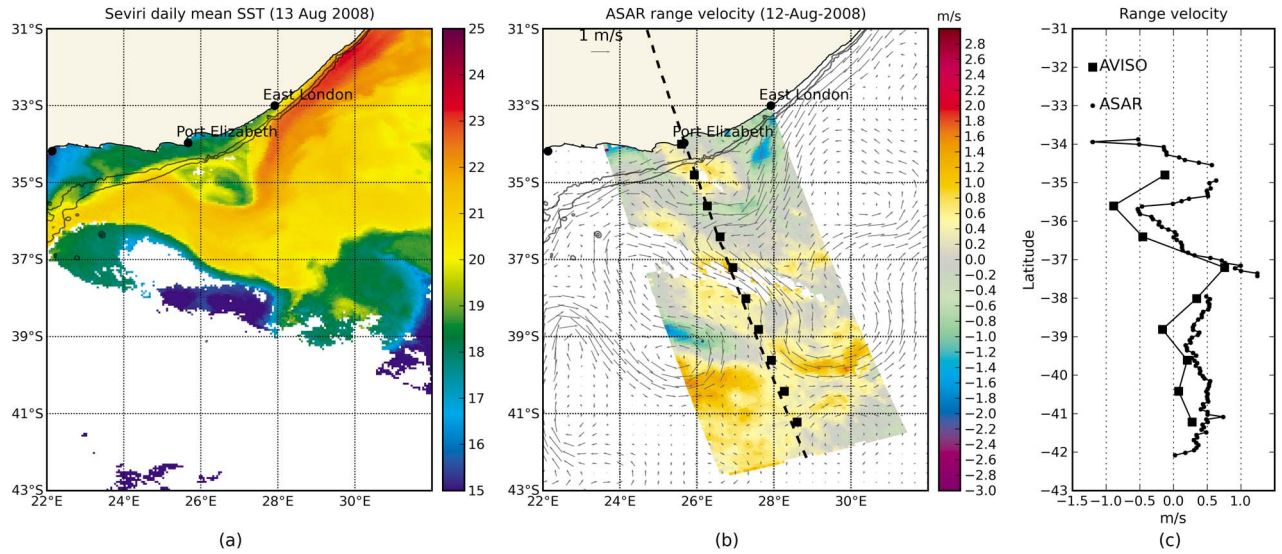

Figure 8. (a and b) Color maps of SST and ASAR range-directed surface current velocity (in m s^{-1}) during the passage of the Natal pulse. Surface temperatures from the Meteosat Second Generation sensor (Figure 8a) show the presence of a cold water core of 150 km diameter at the inshore edge of the Agulhas Current. Figure 8b shows range velocities derived from the ASAR on 12 August 2008 that are overlaid with geostrophic velocity vectors derived from AVISO. Positive values in the color scale indicate a flow toward the northeast. Negative values are associated with a southwesterly flow. (c) A transect taken across the ASAR image illustrates the ability of ASAR and AVISO to capture the presence of a cyclonic flow, with the ASAR providing additional information on the nearshore circulation. Solid black lines in Figures 8a and 8b indicate the position of the 200 m and 1000 m isobaths.

April 2009 and persisted for a period of about 1 month offshore Port Elizabeth were found, in each case, to be associated with the passage of a Natal pulse. Natal pulses have been described as large solitary meanders which move downstream in the Agulhas Current and find their origin in the Natal Bight [*Lutjeharms*, 2006]. Those large perturbations in the Agulhas Current are known to occur at irregular intervals ranging from 50 to 240 days [*De Ruijter et al.*, 1999] and are thought to dominate the annual variability of the Agulhas Current [*Bryden et al.*, 2005]. Natal pulses have an influence on both the local and downstream circulation of the Agulhas Current. Figure 8a shows the surface temperature distribution offshore Port Elizabeth during the passage of the first Natal pulse detected in the time series. Color contours of the ASAR range velocities overlaid with absolute geostrophic currents derived from the merged altimetry around the same period are shown in Figure 8b. The Natal pulse observed around 12 and 13 August 2008 had a diameter of 150 km. It was associated with a cyclonic circulation with a northeastward flow of about 0.5 m s^{-1} along the continental shelf and a southwesterly flow of approximately 0.5 m s^{-1} in the displaced branch of the Agulhas Current. In the SST imagery (Figure 8a), the relatively cooler waters in the center of the eddy were separated from the coastal inshore waters by a warm water plume originating from the Agulhas Current, while the Agulhas Current constituted the offshore boundary of the eddy. The ASAR range velocity map showed that the surface counter flow along the Agulhas Current's inshore edge extended all the way to the coast. Upstream from the trapped border eddy and close to the shore, ASAR range velocities indicated remnants of a southwesterly flow. In situ observations [*Bryden et al.*, 2005] have shown that Natal pulses generate upwelling in the range of 50 m to 100 m near the continental slope. The unique capacity of the Doppler shift method to provide information on the structure of the currents at the coast could be used in the future to better assess the local impact of Natal pulses on the coastal ecosystem. Natal pulses are also thought to play a role in the shedding of Agulhas Rings that move into and across the South Atlantic region [*van Leeuwen et al.*, 2000]. It has been surmised that Natal pulses may at times affect the downstream circulation of the Agulhas Current is such a way as to induce an early retroflection of the Agulhas Current [*Lutjeharms and van Ballegooyen*, 1988]. The Natal pulse observed on 12 August 2008 was the largest anomaly detected in the ASAR data set offshore Port Elizabeth between August 2007 and September 2009 and is thought to have contributed to the early retroflection of the Agulhas Current around September and October 2008.

4. Conclusion

[12] ASAR observations of range-directed surface current velocities derived through the innovative use of the Doppler centroid shift provide a new means of imaging the complex upper ocean dynamics of the Agulhas Current region. The quasi-instantaneous nature of ASAR acquisitions in WSM images combined with the relative high resolution of ASAR range velocity measurements allow synoptic maps of the

Agulhas Current core to be produced for the first time. Comparisons between ASAR- and drifter-derived range velocities showed that inaccuracies in the magnitude of ASAR surface current velocities generally occur when erroneous wind fields are used for the removal of the wind-induced drift on the overall surface motion. The impact of inaccurate wind fields on the quality of the derived surface current velocities is particularly pronounced at low radar incidence angles. As a first approach, it was proposed that only radar incidence angles greater than 30° should be used when computing time-averaged maps of ASAR range velocities. Based on our current understanding of the Agulhas Current system, the time-averaged map of ASAR range velocities seemed able to estimate the mean position and intensity of the Agulhas Current remarkably well. The ASAR range velocities provide a relatively direct and independent mode of observation for monitoring the intensity of the Agulhas Current which could be used to infer interannual fluctuations in the Agulhas Current transport. One of the main findings of this study was to reveal the importance of submesoscale features in shaping the overall variability of the Agulhas Current system. The ability of the ASAR to image fluctuations in the Agulhas Current's path, strength and width, highlight the regions of strong current shear and reveal the occurrence of small shear edge features and eddies, enabled us to show that the magnitude of the variability along the shelf of the Agulhas Bank is comparable to that observed in the Agulhas retroflection. With an improved map of the Agulhas Current variability comes new considerations on the role submesoscale processes play, not only at the local scales which regulate continental shelf exchange, but also on the larger-scale dynamics associated with the Indo-Atlantic exchange. The unique ability of the ASAR range velocities to accurately position regions of strong flow and shear provides new opportunities for oceanographic research in the Agulhas Current and could lead to a better understanding of the Agulhas Current variability, the formation and development of instabilities in the current and the influence of the Agulhas Current on the shelf regions. Significant research effort to improve wind retrieval algorithms from SAR are underway, with the aim of producing wind speed and direction observations independent from the input of existing atmospheric models. The availability of accurate wind observations in the Agulhas Current region would greatly improve the accuracy of ASAR range velocities and could lead to the systematic assimilation of ASAR range velocities in numerical models or to the routine monitoring of Agulhas transport and variability.

[13] **Acknowledgments.** This study was funded by the Earth Observation Unit of the CSIR. Data was provided by ESA through the study contract 18709/05/I-LG. Thanks are given to the radar division of CLS for their support and encouragement during the first author's visit in 2009. The first author also wants to thank the CERSAT for providing the Seviri data set used in this study. Acknowledgement is given to the CHPC for its infrastructure support. Finally, thanks to S. Swart for checking the English of the manuscript.

References

Atlas, D. (1994), Footprints of storms on the sea: A view from spaceborne synthetic aperture radar, *J. Geophys. Res.*, *99*, 7961–7969.

Bryden, H. L., L. M. Beal, and L. M. Duncan (2005), Structure and transport of the Agulhas Current and its temporal variability, *J. Oceanogr.*, *61*, 479–492.

Byrne, D. A., and J. L. McClean (2008), Sea level anomaly signals in the Agulhas Current region, *Geophys. Res. Lett.*, *35*, L13601, doi:10.1029/2008GL034087.

Chang, C., and J. Curlander (1992), Application of the multiple PRF technique to resolve Doppler centroid estimation ambiguity for spaceborne SAR, *IEEE Trans. Geosci. Remote Sens.*, *30*, 941–949.

Chapron, B., F. Collard, and V. Kerbaol (2004), Satellite synthetic aperture radar sea surface Doppler measurements, in *Proceedings of the Second Workshop on Coastal and Marine Applications of SAR*, *Eur. Space Agency Spec. Publ., ESA SP-565*, 133–140.

Chapron, B., F. Collard, and F. Ardhuin (2005), Direct measurements of ocean surface velocity from space: Interpretation and validation, *J. Geophys. Res.*, *110*, C07008, doi:10.1029/2004JC002809.

Cheney, R. A., J. G. Marsh, and B. D. Deckley (1983), Global mesoscale variability from collinear tracks of seasat altimeter data, *J. Geophys. Res.*, *88*, 4343–4354.

Collard, F., A. Mouche, B. Chapron, C. Danilo, and J. A. Johannessen (2008), Routine high resolution observation of selected major surface currents from space, paper presented at Workshop SEASAR 2008, Eur. Space Agency, Frascati, Italy.

De Ruijter, W. P. M., P. J. van Leeuwen, and J. R. E. Lutjeharms (1999), Generation and evolution of Natal pulses: Solitary meanders in the Agulhas Current, *J. Phys. Oceanogr.*, *29*, 3043–3055.

Emery, W. J., C. Fowler, and C. A. Clayson (1991), Satellite-image-derived Gulf Stream currents compared with numerical model results, *J. Atmos. Oceanic Technol.*, *9*, 286–304.

Goldstein, R. M., and H. A. Zebker (1987), Interferometric radar measurement of ocean surface currents, *Nature*, *328*, 707–709.

Grundlingh, M. L. (1983), On the course of the Agulhas Current, *S. Afr. Geog. J.*, *65*, 49–57.

Harris, T. F. W., R. Legeckis, and D. van Forest (1978), Satellite infra-red images in the Agulhas Current system, *Deep Sea Res.*, *25*, 543–548.

Horstmann, J., W. Koch, and S. Lehner (2004), Ocean wind fields retrieved from the advanced synthetic aperture radar aboard Envisat, *Ocean Dyn.*, *54*, 570–576.

Johannessen, J. A., V. Kudryavtsev, D. Akimov, T. Eldevik, N. Winther, and B. Chapron (2005), On radar imaging of current features: 2. Mesoscale eddy and current front detection, *J. Geophys. Res.*, *110*, C07017, doi:10.1029/2004JC002802.

Johannessen, J. A., B. Chapron, F. Collard, V. Kudryavtsev, A. Mouche, D. Akimov, and K. F. Dagestad (2008), Direct ocean surface velocity measurements from space: Improved quantitative interpretation of Envisat ASAR observations, *Geophys. Res. Lett.*, *35*, L22608, doi:10.1029/2008GL035709.

Koshlyakov, M. N. (1986), Eddies of western boundary currents, in *Synoptic Eddies in the Ocean*, pp. 208–264, D. Reidel, Dordrecht, Holland.

Largier, J., P. Chapman, W. T. Peterson, and V. P. Swart (1992), The western Agulhas Bank: Circulation, stratification and ecology, *S. Afr. J. Mar. Sci.*, *12*, 319–339.

Lee, T., L. Atkinson, and R. Legeckis (1981), Observations of a Gulf Stream frontal eddy on the Georgia continental shelf, *Deep Sea Res., Part A*, *28*, 347–378.

Lutjeharms, J. R. E. (2006), *The Agulhas Current*, Springer, Berlin.

Lutjeharms, J. R. E., and R. C. van Ballegooyen (1988), Anomalous upstream retroflection in the Agulhas Current, *Science*, *240*, 1770–1772.

Lutjeharms, J., R. Catzel, and H. R. Valentine (1989), Eddies and other boundary phenomena of the Agulhas Current, *Cont. Shelf Res.*, *9*, 597–616.

Lutjeharms, J., P. Penven, and C. Roy (2003), Modelling the shear edge eddies of the southern Agulhas Current, *Cont. Shelf Res.*, *23*, 1099–1115.

Madsen, K. S., J. L. Hyer, and C. C. Tscherning (2007), Near-coastal satellite altimetry: Sea surface height variability in the North Sea–Baltic Sea area, *Geophys. Res. Lett.*, *34*, L14601, doi:10.1029/2007GL029965.

Madsen, S. N. (1989), Estimation the Doppler centroid of SAR data, *IEEE Trans. Aerosp. Electron. Syst.*, *25*, 134–140.

Mouche, A., B. Chapron, N. Reul, and F. Collard (2008), Predicted Doppler shifts induced by ocean surface displacements using asymptotic electromagnetic wave scattering theories, *Waves Random Complex Media*, *18*, 185–196.

Niiler, P. P., N. A. Maximenko, and J. C. McWilliams (2003), Dynamically balanced absolute sea level of the global ocean derived from near-surface velocity observations, *Geophys. Res. Lett.*, *30*(22), 2164, doi:10.1029/2003GL018628.

Pearce, A. F., and M. L. Grundlingh (1982), Is there a seasonal variation in the Agulhas Current?, *J. Mar. Res.*, *40*, 177–184.

Penven, P., J. R. E. Lutjeharms, P. Marchesiello, C. Roy, and S. J. Weeks (2001), Generation of cyclonic eddies by the Agulhas Current in the lee of the Agulhas Bank, *Geophys. Res. Lett.*, *27*, 1055–1058.

Portabella, M., A. Stoffelen, and J. Johannessen (2002), Toward on optimal inversion method for synthetic aperture radar wind retrieval, *J. Geophys. Res.*, *107*(C8), 3086, doi:10.1029/2001JC000925.

Probyn, T. A., B. Mitchell-Innes, and S. Searson (1995), Primary productivity and nitrogen uptake in the subsurface chlorophyll maximum on the eastern Agulhas Bank, *Cont. Shelf Res.*, *15*, 1903–1920.

Rio, M.-H., and F. Hernandez (2004), A mean dynamic topography computed over the world ocean from altimetry, in situ measurements, and a geoid model, *J. Geophys. Res.*, *109*, C12032, doi:10.1029/2003JC002226.

Rio, M.-H., P. Schaeffer, J.-M. Lemoine, and F. Hernandez (2005), Estimation of the ocean mean dynamic topography through the combination of altimetric data, in-situ measurements and GRACE geoid: From global to regional studies, paper presented at GOCINA international workshop, Cent. Eur. de Geodyn. et de Seismol., Kirchberg, Luxembourg.

Rio, M.-H., P. Schaeffer, G. Moreaux, J.-M. Lemoine, and E. Bronner (2009), A new mean dynamic topography computed over the global ocean from GRACE data, altimetry and in-situ measurements, poster presented at OceanObs09 Conference, Eur. Space Agency, Venice, Italy, 21–25 Sept.

Romeiser, R., H. Breit, M. Eineder, H. Runge, P. Flament, K. de Jong, and J. Vogelzang (2005), Current measurements by SAR along-track interferometry from a space shuttle, *IEEE Trans. Geosci. Remote Sens.*, *43*, 2315–2324.

Shemer, L., M. Marom, and D. Markman (1993), Estimates of currents in the nearshore ocean region using interferometric synthetic aperture radar, *J. Geophys. Res.*, *98*, 7001–7010.

Siedler, G., M. Rouault, and J. R. E. Lutjeharms (2006), Structure and origin of the Subtropical South Indian Ocean Countercurrent, *Geophys. Res. Lett.*, *33*, L24609, doi:10.1029/2006GL027399.

Stoffelen, A., and D. Anderson (1997), Scatterometer data interpretation: Estimation and validation of the transfer function cmod4, *J. Geophys. Res.*, *102*, 5767–5780.

U.S. Department of Commerce (2004), *Synthetic Aperture Radar Marine User's Manual*, edited by C. R. Jackson and J. R. Apel, Nat. Oceanic and Atmos. Admin., Silver Spring, Md.

Vachon, P., and F. Dobson (1996), Validation of wind vector retrieval from ERS-1 SAR images over the ocean, *Global Atmos. Ocean Syst.*, *5*, 177–187.

van der Vaart, P. C. F., and W. P. M. de Ruijter (2001), Stability of western boundary currents with an application to pulselike behavior of the Agulhas Current, *J. Phys. Oceanogr.*, *31*, 2625–2644.

van Leeuwen, P. J., W. P. M. de Ruijter, and J. R. E. Lutjeharms (2000), Natal pulses and the formation of Agulhas Rings, *J. Geophys. Res.*, *105*, 6425–6436.

Vianna, M. L., V. V. Menezes, and D. P. Chambers (2007), A high resolution satellite-only GRACE-based mean dynamic topography of the South Atlantic Ocean, *Geophys. Res. Lett.*, *34*, L24604, doi:10.1029/2007GL031912.

Vignudelli, S., P. Berry, and L. Roblou (2008), Satellite altimetry near coasts—Current practices and a look at the future, paper presented at 15 Years of Progress in Radar Altimetry, Eur. Space Agency, Venice, Italy.

B. Chapron, IFREMER, F-29280 Plouzané, France.

F. Collard and A. Mouche, Direction of Radar Applications, CLS, 115, rue Claude Chappe, F-29280 Plouzané, France.

J. A. Johannessen, Nansen Environmental and Remote Sensing Center, Thormoehlensgate 47, N-5006 Bergen, Norway.

M. J. Rouault, Ecosystem Earth Observation, Council for Scientific and Industrial Research, 15 Lower Hope St., Cape Town, 7700 South Africa. (mrouault@csir.co.za)